

A Multi-scale Transformer for Medical Image Segmentation: Architectures, Model Efficiency, and Benchmarks

Yunhe Gao¹Mu Zhou²Di Liu¹Dimitris Metaxas¹

Abstract—Transformers have emerged to be successful in a number of natural language processing and vision tasks, but their potential applications to medical imaging remain largely unexplored due to the unique difficulties of this field. In this study, we present UTNetV2, a simple yet powerful backbone model that combines the strengths of the convolutional neural network and Transformer for enhancing performance and efficiency in medical image segmentation. The critical design of UTNetV2 includes three innovations: (1) We used a hybrid hierarchical architecture by introducing depthwise separable convolution to projection and feed-forward network in the Transformer block, which brings local relationship modeling and desirable properties of CNNs (translation invariance) to Transformer, thus eliminate the requirement of large-scale pre-training. (2) We proposed efficient bidirectional attention (B-MHA) that reduces the quadratic computation complexity of self-attention to linear by introducing an adaptively updated semantic map. The efficient attention makes it possible to capture long-range relationship and correct the fine-grained errors in high-resolution token maps. (3) The semantic maps in the B-MHA allow us to perform semantically and spatially global multi-scale feature fusion without introducing much computational overhead. Furthermore, we provide a fair comparison codebase of CNN-based and Transformer-based on various medical image segmentation tasks to evaluate the merits and defects of both architectures. UTNetV2 demonstrated state-of-the-art performance across various settings, including large-scale datasets, small-scale datasets, 2D and 3D settings.

I. INTRODUCTION

Transformer architectures emerge as a visual representation backbone in a variety of computer vision applications. Unlike convolutional neural networks (CNNs), Transformer uses attention-based operations for data modeling to achieve promising performance [1]. Growing findings have shown that vision Transformers can exhibit higher capacity than CNNs under large-scale training [1]. However, due to the lack of inductive bias, the vision Transformer does not generalize well on small-scale data [2]. Therefore, applying Transformer to medical image segmentation is particularly challenging as we are often given limited disease-specific medical imaging cohorts.

We need to address multiple data-centric difficulties in computational medical image segmentation: (1) Image-based tasks often come with only small amount of available samples due to disease subtypes, data modalities, acquisition difficulties, privacy issues and high annotation costs, which makes it difficult for large-scale training or pre-training. (2)

¹ Yunhe Gao, Di Liu and Dimitris Metaxas are with Department of Computer Science, Rutgers University, Piscataway, New Jersey, USA. yunhe.gao@rutgers.edu

² Mu Zhou is with the SenseBrain Research, Princeton, New Jersey, USA.

Due to the imaging principle, the boundary of the region of interest is not necessarily clear, thus contextual information is vital to help reasoning. (3) The size of different organs or lesions in the body varies greatly, and it is necessary to fuse high-resolution low-level features and low-resolution high-level features to help delineate the detailed boundary.

In this study, we first analyze the merits and defects of the Transformer and CNN architectures. Self-attention is the core computational primitive in Transformer to capture long-range associative features by implementing pairwise entity interactions with a context aggregation mechanism. It also allows the model to aggregate features dynamically based on the input content. Although Transformers might have potentially higher model capacity, it requires a large amount of training data due to the lack of inductive bias. Moreover, the global all-to-all attention has a quadratic complexity with respect to the input size, which is unacceptable for high-resolution inputs, especially for 3D data. On the other hand, CNNs use convolution to gather information within the kernel footprint in a sliding window strategy. This locality introduces inductive bias such as translation invariance to the CNN models, enabling the model to quickly converge on small-scale data while significantly reducing the amount of computation for high-resolution input. However, this locality also brings local receptive fields, which makes CNN unfavorable to explicit long-range relationship modeling [3]–[5]. Both CNN and Transformer architectures have presented their unique advantages, an integrative analysis combining the strength of two architectures is of substantial interest.

Currently, preliminary studies have attempted to apply Transformer in the medical image segmentation field [6]–[9]. A common strategy is to apply vision Transformer directly (e.g., ViT [1], or SwinTransformer [10]) into medical image analysis. These efforts rely on advanced training techniques on top of the Transformer model, including more data augmentations and longer training epochs. However, in our experiments, we found that if the same advanced training techniques are applied to CNNs, CNNs can achieve comparable or even better performance than standard Transformer models as confirmed as well in [11], [12].

In this paper, we elaborately design a hybrid model to address the difficulties of medical image segmentation, which is an improved version of U-shape hybrid Transformer Network: **UTNetV2**. The contribution of this paper lies in four folds:

- We propose a hybrid hierarchical architecture for 2D and 3D medical image segmentation. Specifically, we introduce depth-wise separable convolution into the pro-

jection of attention and the feed-forward network in the Transformer block to introduce convolution inductive bias to Transformer, which allows our model to be trained from scratch in the small-scale medical dataset without any pre-training weights.

- We proposed an efficient bidirectional multi-head attention (B-MHA) that reduces the quadratic complexity of conventional self-attention to linear. The B-MHA learns to non-linearly compress the large token map to a small semantic map which preserve the most useful tokens while discard redundant ones.
- We propose a semantically and spatially global multi-scale fusion mechanism based on the semantic map to enhance the segmentation without introducing remarkable computation overhead.
- Extensive experiments are performed, including large-scale to small-scale datasets, 2D and 3D settings, to demonstrate the effectiveness of the proposed method.
- We provide an easy-to-use codebase¹ as a benchmark for fair comparison between CNN and Transformer architectures in a variety of medical image segmentation tasks, which contains the code for the model, configuration, data processing and training framework used in this work.

II. RELATED WORK

In this section, we discuss and review related topics of medical image segmentation from three aspects: CNN models, vision Transformer-based models and multi-scale feature fusion.

A. CNNs for medical image segmentation

Using convolution as the basic operator, CNNs collect local response within a local footprint and filter the image in a sliding window manner, which is intrinsic to many visual processing scenarios. The local connection and weight sharing greatly reduce the computation complexity, number of parameters and introduce built-in inductive bias to CNNs, such as translation equivalence. These advantages enable CNNs to be efficient on high-resolution images, and to obtain fast convergence and good performance on small-scale data. Nevertheless, this locality also leads to a limited receptive field, which makes CNN unable to effectively model long-distance relationships directly. Thus CNN models need to stack multiple convolutional layers and down-sampling layers to gradually increases the receptive field and extract higher-level features hierarchically.

The fully-convolutional network (FCN) [13] is an early attempt which computes low-resolution representations to estimate a coarse segmentation map and uses intermediate medium-resolution segmentation score maps for refinement. UNet [14] proposes a symmetric encoder-decoder architecture which gradually recovers the high-resolution representations from the low-resolution representations by up-sampling and concatenating features from encoder via

skip connections. Although down-sampling can effectively expand the range of the receptive field, it also reduces the resolution and loses detailed information. Therefore, some works attempt to expand the receptive field of medium-resolution representation through dilated convolutions [15], [16], or fuse multi-scale representations via input pyramid [17], feature pyramid [3], [18], [19], or dense skip connections [20], [21]. Attention [22] and self-attention [23], [24] mechanism are also incorporated to help CNN to model long-range dependencies and make model focus on the region of interests. A vast number of works based on variants of FCN and UNet are applied in the 2D and 3D medical image segmentation field [25]–[29].

B. Vision Transformer and variants

Transformer models with attention mechanism as the core operator are emerging in vision tasks. The self-attention module computes an all-to-all attention matrix to adaptively update representations from all input tokens, which inherently has a global receptive field to model long-range relationship. ViT [1] is the first work based on a pure Transformer architecture to surpass CNNs in image classification under large-scale training. ViT divides images into non-overlapping patches which are then projected into embedding space as a sequence of tokens. Multiple standard Transformer layers including multi-head self-attention (MHSA), position-wise feed-forward network (FFN) are applied to model these tokens.

Due to the quadratic complexity of self-attention with respect to the input sequence length, ViT has to divide the image into medium-size patches as tokens to reduce computation. This patchify operation can be regarded as an aggressive down-sampling operation, which discards all structural information within the patch. This might be acceptable for classification, but it would be terrible in dense prediction tasks such as segmentation, as a large amount of detailed information will be lost [10]. Moreover, due to the lack of CNN’s inductive bias, ViT is still not as good as CNN when the amount of data is small [2], which is the common case in medical image analysis field. Thus the improvement of vision Transformer are either improving the structure for better performance and reducing the requirement of training data, or improving the efficient and reduce the computation complexity.

Several works attempt to introduce inductive bias back to Transformer. CVT [30] uses a hierarchical structure and replace the linear embedding and projection with convolutional embedding and projection, which bring convolution inductive bias to the ViT architecture. CoAtNet [2] presents a family of hybrid models that unify depthwise convolution and self-attention via relative attention and finds vertically stacking convolution layers and attention layers in a principled way can improve generalization, capacity and efficiency. These two methods outperform ViT when training on relatively small ImageNet-1k dataset.

To reduce the computation complexity, recent works develop three main directions: (1) Local window self-attention.

¹<https://github.com/yhygao/CBIM-Medical-Image-Segmentation>

SwinTransformer [10] introduces the locality of convolution into self-attention via non-overlap window-based multi-head self-attention (W-MSA). (2) Decomposing attention. CCNet [24] propose a criss-cross module to decompose 2D attention to two 1D attention. This idea is also applied in [31]. (3) Reduce the number of tokens. As images are highly-structured data, redundancy exists among tokens. UTNet [32] and concurrent work CvT [30], PvT [33] attempt to reduce the tokens in key and value to improve efficiency.

For the first two directions, although they greatly reduce the complexity, the locality or decomposing brings the defect of limited receptive field and worse capability to directly model long-range relationship. For example, to propagate information across windows, SwinTransformer has to apply two shifted-window self-attentions in the consecutive layers. CCNet requires to recurrently stack multiple criss-cross modules to aggregate full dependencies. The proposed UTNetV2 lies in the third direction, where the key is how to retain useful tokens while eliminate redundant tokens.

There are several attempts to apply Transformer in the medical image segmentation field. TransUNet [6] and UNETR [8] add 2D or 3D decoder to ViT-like encoder and proves Transformer can be applied in medical image segmentation in 2D and 3D setting. SwinUNet [7] and VT-UNet [9] use SwinTransformer-like encoder-decoder structure for 2D and 3D segmentation. These models usually need to be initialized with pre-trained weights on large-scale natural image datasets and longer training epochs, otherwise they achieve poor performance on smaller medical image datasets.

C. Multi-scale feature fusion

Multi-scale feature fusion is widely studied and proven to be effective for dense prediction tasks [15], [34], [35]. A straightforward way is to resample the input images into multi-resolution input pyramid and feed into multiple or shared networks then aggregate the output [36]–[38]. UNet [14] concatenate up-sampled high-level feature from decoder with low-level feature from encoder skip connections to gradually fuse multi-scale features. Some approach propose to add more connections between high- and low-level representations for multi-scale fusion, e.g. UNet++ [20] adds nested skip connections from high-level to low-level representations. HRNet [39] adds full connections among high- and low-level representations. Feature pyramid fuses multi-scale feature by pyramid pooling [3] or atrous spatial pyramid pooling [19].

The above-mentioned methods usually interpolate the features of different scales to the same size, and then uses convolution to fuse the semantic features of different scales at same position, which is spatially local fusion. For example, the multi-scale features of the object in the upper left corner of the image will not help the same object in the lower right corner. Our proposed semantic map based multi-scale fusion is global fusion spatially and semantically. Any position of different scale features can help each other. Due to the smaller size of the semantic map, this global fusion brings even negligible computation overhead.

III. METHOD

A. Overall Architecture

An overview of the architecture of UTNetV2 is shown in Fig. 1 (a). It first models the local features of the image and embeds them into token map through a convolution stem, which stack multiple convolution layers and down-sampling to reduce the spatial resolution to $4 \times$ down-samplings. Since the high-resolution features are important for the boundary. These $1 \times$ and $2 \times$ high-resolution features in the Convolution stem are then feed to the decoder through skip connections.

A concise semantic map is generated from the token map. Several proposed bidirectional (B-MHA) Transformer blocks are applied to process the token map and the semantic map. To generate a hierarchical representation, we reduce the size of the token map by down-sampling, which is achieved by a patch merging layer [10]. B-MHA blocks are applied on the down-sampled $8 \times$ token map, then the same for the $16 \times$ level. In this way, we obtain token maps of multiple scales hierarchically, as well as their corresponding compressed semantic maps. We fuse the information of the multi-scale semantic map through a multi-scale fusion module, which is very efficient due to the small size of the semantic map. Then, we gradually restore the resolution through up-sampling in the decoder. At each level, the token map from the encoder, as well as the corresponding fused semantic map, will be concatenated via skip connections and then processed by the B-MHA blocks. At last, a convolutional decoder combines the high-resolution feature maps from the convolutional stem to output the final segmentation map.

UTNetV2 uses CNN stem to extract local features in the shallow layer, and then enhances the long-distance and local features through the proposed bidirectional transformer block. At the same time, it can efficiently integrate multi-scale information, so it can replace various UNet variants and become a general segmentation backbone.

In the following section, we aim at explaining the idea behind UTNetV2 by answering the following two questions: (1) How to combine the strength of CNN and Transformer such that it has large model capacity as well as inductive bias that don't require large amount training data. (2) How to design an efficient yet effective attention module that is suitable for medical image segmentation task. (3) How to better fuse multi-scale information for semantic segmentation. We'll introduce the proposed approach in 2D version for simplicity, while it can be easily extended to 3D version.

B. Preliminary

The Transformer is built upon the multi-head self-attention (MHSAs) module and feed-forward network (FFN) [40].

Attention Module. For vision tasks, given a representation map $X \in \mathcal{R}^{d \times H \times W}$, where H, W are the spatial height, width and d is the number of channels, where every pixel is treated as a token. The token map is flatten to a sequence as the input of the Transformer block: $\mathbf{X} \in \mathcal{R}^{n \times d}$ (bold for flattened 1D sequence, while regular for 2D token map), where $n = HW$ is the sequence length. Three linear

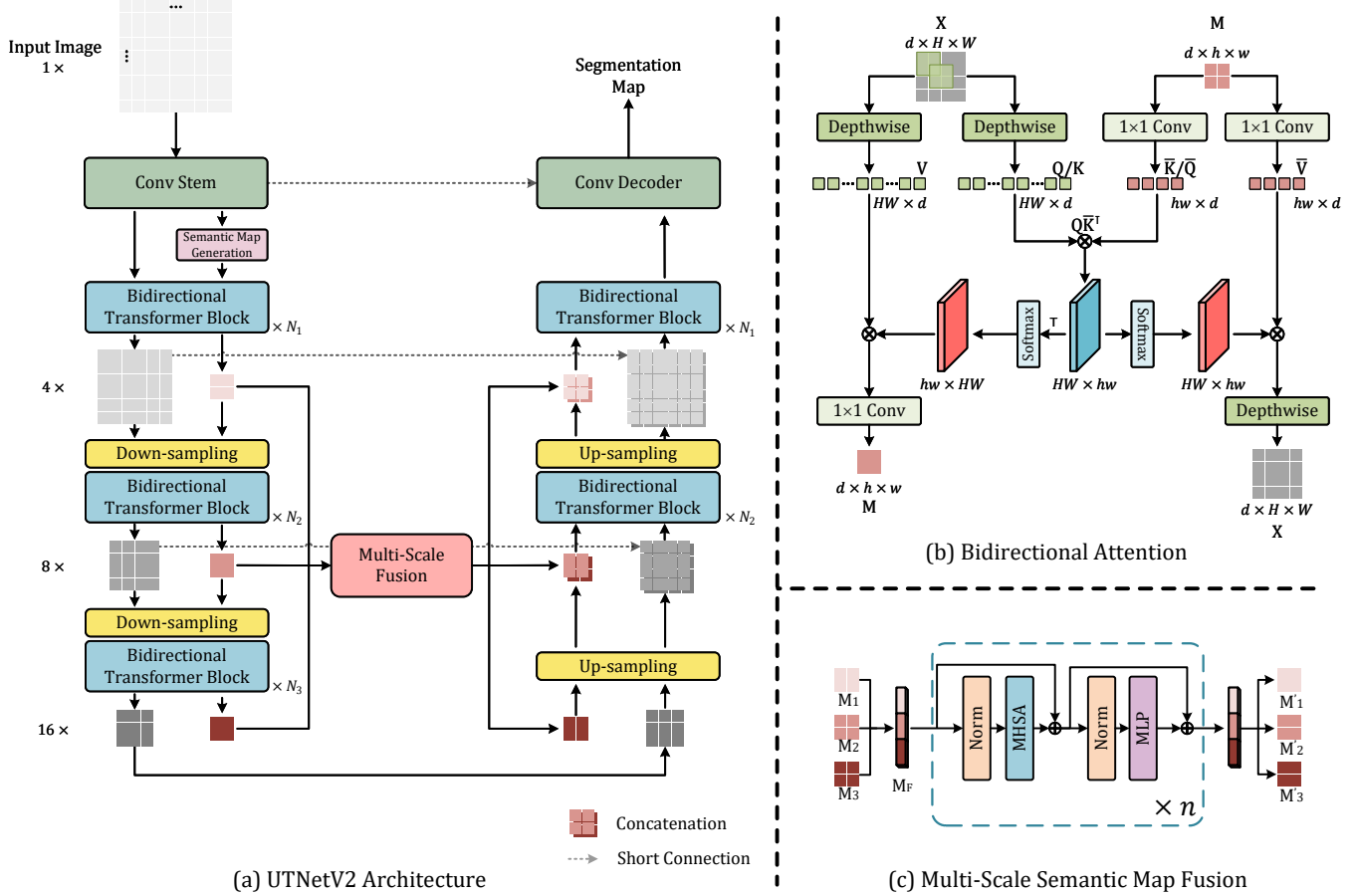


Fig. 1. The illustration of overall framework

transformations are used to project \mathbf{X} to query, key and value embeddings: $\mathbf{Q}, \mathbf{K}, \mathbf{V} \in \mathcal{R}^{n \times d}$. The scaled dot-product attention used by Transformer is given by:

$$\text{Attention}(\mathbf{Q}, \mathbf{K}, \mathbf{V}) = \underbrace{\text{softmax}\left(\frac{\mathbf{Q}\mathbf{K}^T}{\sqrt{d}}\right)}_{\mathbf{A}} \mathbf{V} \quad (1)$$

$\mathbf{A} \in \mathcal{R}^{n \times n}$ is often called attention matrix that measures the similarity of each token-pairs as weights for aggregate context information from value embedding. Instead of applying the single-head attention, Transformer uses multi-head self-attention that project the query, key and value embeddings to multiple representation sub-spaces for attention computation. Outputs of multiple heads are concatenated as the final output for better capacity as well as reduce overfitting. We omit the multi-head in all formulas in this paper for simplicity.

Feed-forward network. The FFN is a position-wise two-layer perceptron that consists of two linear layers and activation functions that operates separately and identically on each position. FFN works as feature transformation layer that increases model capacity by introducing non-linear transformation.

C. Convolutional Projection and Feed-forward Network

The position-wise linear projection for attention module and the FFN in vanilla Transformer block only transforms the tokens element-wise without interacting with other tokens. This makes the Transformer to be permutation invariant and discard all local structure information that is vital for images. Although adding positional encoding allows the Transformer to learn position relationship, learning from scratch demands a huge amount of training data, which is a key pain point of medical image analysis.

Therefore, we propose to introduce convolution to the projection of attention and the feed-forward network, see in Fig. 1 (b). Given a 2D token map \mathbf{X} , a convolution with kernel size k is implemented to project the feature map into different spaces and are then flattened into 1D for subsequent attention computation as query, key or value. This can be formulated as:

$$\mathbf{Q}/\mathbf{K}/\mathbf{V} = \text{Flatten}(\text{Conv}(\mathbf{X}, k)) \quad (2)$$

We use the depth-wise separable convolution [41] as an efficient version of convolution which is implemented by: depthwise conv \rightarrow pointwise conv, where the depth-wise convolution gathers the spatial information while the pointwise convolution gathers along the channel dimension.

For FFN, we adopted a similar modification. Given token sequence \mathbf{X} after attention module, we first reshape them back to 2D and transform them with convolutional blocks:

$$X = \text{ConvBlock}(\text{Reshape2D}(\mathbf{X}), k) \quad (3)$$

We use the MBCConv [42] as the convolutional blocks, which consists of: depthwise conv \rightarrow activation \rightarrow pointwise conv. The proposed convolutional projection and feed-forward network is a generalized version of the origin Transformer design, which can be implemented using 1×1 convolution layer in both modules.

D. Efficient Bidirectional Attention

Efficient Attention. The computation bottleneck of vision Transformer comes from the attention module. The dot-product of two $n \times d$ matrices leads to $O(n^2d)$ complexity. Typically, the sequence length n is much larger than d in vision tasks when the resolution of token map is high, especially for 3D tasks, thus dominates the self-attention computation and makes it infeasible to apply self-attention in high-resolution token maps.

As images are highly structured data, most pixels in high-resolution feature maps within local footprint share similar semantic meanings. Therefore, the all-to-all attention is highly inefficient and redundant. From a theoretical perspective, self-attention is essentially low rank for long sequences [43], which indicates that most information is concentrated in the largest singular values. Inspired by this finding, UTNetV1 [32] proposed an efficient self-attention mechanism by reducing the number of tokens in key and value through sub-sampling, similar idea is also applied in concurrent work [30], [33].

The main idea is to use two projections to reduce the number of tokens in key and value: $\mathbf{K}, \mathbf{V} \in \mathcal{R}^{n \times d}$ to: $\bar{\mathbf{K}}, \bar{\mathbf{V}} \in \mathcal{R}^{l \times d}$, where $l = hw \ll n$, h and w are the reduced size of token map after sub-sampling. The efficient self-attention is:

$$\text{Attention}(\mathbf{Q}, \bar{\mathbf{K}}, \bar{\mathbf{V}}) = \text{softmax}\left(\frac{\mathbf{Q}\bar{\mathbf{K}}^T}{\sqrt{d}}\right) \underbrace{\bar{\mathbf{V}}}_{\bar{A}:n \times l} \quad (4)$$

By doing so, the computational complexity is reduced to $O(nld)$, which is linear to the input sequence length n .

Bidirectional Attention (B-MHA). Although the mentioned efficient attention can greatly reduce the amount of computation, it is still sub-optimal. The key idea is how to reduce the number of token such that useful tokens are retained while redundant tokens are discarded. For the concern of computation, the down-sampling methods in current efficient attention are simple linear transformation, such as interpolation, or strided convolution. These simple linear operations don't have a global point of view and cannot guarantee the most informative tokens are preserved when compression ratio is high.

Therefore, we proposed a bidirectional multi-head attention module (B-MHA) that maintains a semantic map to store

the low-dimensional token map by non-linear dimensionality reduction, see in Fig. 1 (b). To be specific, an initial semantic map which has a much smaller spatial size is generated after the convolutional stem by using a linear transformation. The B-MHA module has two inputs, one is the conventional token map X from the previous layer, while another is the semantic map M . The X and M are projected to $\mathbf{Q}/\mathbf{K}/\mathbf{V}$ and $\bar{\mathbf{Q}}/\bar{\mathbf{K}}/\bar{\mathbf{V}}$ respectively for a cross-attention. Note that the X is projected with depthwise separable convolution while M is projected with 1×1 convolution. It's because the M has much smaller size and each element in M has valuable semantic information, the padding in 3×3 depthwise convolution will introduce noise to the semantic map. To reduce the computation as well as memory consumption, query and key of X and M are shared. As the dot product of query and key measures the similarity of a token-pair, which is symmetrical, we can reuse it for compute the attention matrix to aggregate context for both X and M by simply transpose the dot product matrix (before softmax):

$$\begin{aligned} X &= \text{Attention}(\mathbf{Q}, \bar{\mathbf{K}}, \bar{\mathbf{V}}) = \text{softmax}\left(\frac{\mathbf{Q}\bar{\mathbf{K}}^T}{\sqrt{d}}\right)\bar{\mathbf{V}} \\ M &= \text{Attention}(\bar{\mathbf{Q}}, \mathbf{K}, \mathbf{V}) = \text{softmax}\left(\frac{\bar{\mathbf{Q}}\mathbf{K}^T}{\sqrt{d}}\right)\mathbf{V} \\ \bar{\mathbf{Q}}\mathbf{K}^T &= (\mathbf{Q}\bar{\mathbf{K}}^T)^T \end{aligned} \quad (5)$$

Compared with linear down-sampling, the non-linear update of semantic map in the B-MHA makes it has better capability in dimension reduction for better compression. Furthermore, the low-dimension information in the semantic map is not discarded as in the efficient attention, but is continuously updated and improved. The semantic map works as a global summary of the high-dimensional token map. This mechanism allows the attention module to directly aggregate global context information, while consume a much smaller computation. Also, the depthwise separable convolution in the projection and FFN is complementarily good at capturing local response which makes the proposed B-MHA Transformer block to be excellent in the modeling of both local and global relationships.

Complexity. The computation complexity comparison of convolutional layer and different attention modules are shown in Table I. Given a feature representation map with size $d \times H \times W$ and a semantic map with size $d \times h \times w$, where $h, w \ll H, W$ are fix values. The Convolutional layers, shifted-window (Swin) self-attention and the proposed B-MHA have linear complexity to the input length HW , while the vanilla self-attention has quadratic complexity which is unaffordable for high-resolution feature maps. Note that the SwinTransformer needs to consecutively stack a window-based self-attention and a shifted-window self-attention to model connections across windows, so the complexity and parameters are doubled.

E. Multi-scale Semantic Map Fusion

Multi-scale fusion plays a vital role in dense prediction tasks to combine the high-level semantic information and

TABLE I
THE COMPUTATION COMPLEXITY COMPARISON.

Module	Complexity	parameters
Conv	$\Omega(k^2 H W d^2)$	$k^2 d^2$
MHSA	$\Omega(4 H W d^2 + 2(HW)^2 d)$	$4d^2$
W-MHA+SW-MHA [10]	$\Omega(8 H W d^2 + 4M^2 H W d))$	$8d^2$
B-MHA	$\Omega(3 H W d^2 + 3h w d^2 + 3h w H W d)$	$6d^2$

k : convolution kernel size, HW : the input token number, d : token dimension, M : the window size of shifted-window (Swin) self-attention, $h w$: the semantic map token number.

low-level detailed information when recover the resolution. The semantic map in B-MHA is naturally suitable for multi-scale fusion with a small amount of computation. See in Fig. 1 (c), given 2D semantic maps from multiple scales: M_1, M_2, \dots, M_n , we first flatten them and concatenate them together into a long 1D token sequence: $\mathbf{M}_F = \text{Concat}(\text{Flatten}(M_1), \text{Flatten}(M_2), \dots, \text{Flatten}(M_n))$. The sequence \mathbf{M}_F that contains all tokens from all scales is then feed into conventional Transformer blocks which consists of multi-head self-attention and feed-forward network for multi-scale semantic fusion. The fused sequence is then chunked and reshaped back to 2D semantic maps. The semantic map is a summary of the full feature map which contains rich semantic information of the corresponding scale. The MHSA in Transformer block can model the relationship among tokens at any position across all scales, which push the multi-scale fusion to extreme: global fusion both semantically and spatially.

IV. EXPERIMENTS

Our comparative experiment mainly wants to answer two questions: (1) The impact of the amount of training data on CNN and Transformer. (2) In different segmentation tasks, the fair performance comparison of CNN and Transformer models under the same training techniques.

A. Datasets

For the first question, we collected a large cardiac MRI data set which consists of total 1418 MRI scans. We train all models with 5%, 10%, 40%, 70% and 100% of the dataset and test their performance. For the second question, we evaluate all models on ACDC cardiac MRI segmentation and BTCV abdominal organ CT segmentation dataset, respectively.

The collected large short-axis cardiac MRI dataset includes ACDC, M&Ms, M&Ms-2, and UK Biobank (UKBB). These four dataset have the same annotation with left ventricle (LV), right ventricle (RV) and left ventricular myocardium (MYO). The training set includes 100 ACDC cases, 150 M&Ms cases, 160 M&Ms-2 cases, and 1008 UKBB cases, which is totally 1418 MRI scans. We used the M&Ms test set as our test set, which contains 170 scans from 4 manufacture vendors.

The UK Biobank (UKBB) is a population-based prospective study established to allow detailed investigations of the genetic and environmental determinants of the diseases, whose cohort consists of 500,000 voluntary participants, with ages ranging between 40 and 69 years, that were

recruited between 2006 and 2010 across the UK. Starting from 2014, 100,000 volunteers from the whole cohort were also enrolled for multi-modal imaging, including MR of the brain, the heart and the full body. In this work, 1008 short-axis cardiac MR images from UKBB, which are performed in a multi-centre setting using standardised protocols, are used as training data. As UKBB is a prospective study, these patients do not necessarily have heart disease.

The ACDC dataset (Automated Cardiac Diagnosis Challenge) [44] contains cardiac short-axis Cine MRI data from 100 patients collected from University Hospital of Dijon (France), which includes healthy patients, patients with previous myocardial infarction, dilated cardiomyopathy, hypertrophic cardiomyopathy, and abnormal right ventricle, 20 scans for each group. These data are obtained over a 6 year period using two MRI scanner of two magnetic strength (1.5T and 3.0T). A series of short axis slices cover the LV from the base to the apex, with a thickness of 5-10 mm. The spatial resolution goes from 0.70 to 1.92 mm^2 /pixel and 28 to 40 images cover completely or partially the cardiac cycle.

The M&Ms (Multi-centre, multi-vendor and multi-disease cardiac segmentation) [45] and M&Ms-2 are challenges in conjunction with MICCAI and STACOM. The M&Ms challenge cohort includes patients with hypertrophic and dilated cardiomyopathies as well as healthy subjects. All subjects were scanned in clinical centres in three different countries (Spain, Germany and Canada) using four different MRI scanner vendors (Siemens, General Electric, Philips and Canon). The training set contains 150 annotated images from two vendors (75 each), while the testing set contains 170 cases (20 for the first vendor and 50 each for other three vendors). The M&Ms-2 cohort was collected in three clinical centres from Spain using three different magnetic resonance scanner vendors (Siemens, General Electric and Philips). The training set contains 160 annotated images, including 40 normal subjects, 30 dilated left ventricle subjects, 30 hypertrophic cardiomyopathy subjects, 20 congenital arrhythmogenesis subjects, 20 tetralogy of fallot and 20 interatrial communication subjects.

The BTCV dataset (Multi-Atlas Labeling Beyond the Cranial Vault) [46] consists of 30 subjects with abdominal CT scans where 13 organs were annotated by interpreters under supervision of radiologists at Vanderbilt University Medical Center. Each CT scan was acquired with contrast enhancement in portal venous phase and consists of 80 to 225 slices with 512×512 pixels and slice thickness ranging from 1 to 6 mm.

B. Experimental Settings

1) *Implementations*: For data preprocessing, we basically followed the setting of nnUNet [47]. For a 2D model, the in-plane of all images is first resampled to the median spacing of the entire dataset, while the through-plane spacing remains unchanged. For 3D models, images are resampled to the median spacing of in all three axis. Images are then normalized according to the intensity of the foreground. In evaluation, the 2D models take the image slices as input,

while the 3D models inference using sliding window with half window overlap. The size of semantic map of UTNetV2 is usually half the size of the lowest resolution token map. The dimension of semantic map is consistent with the token map in the same level.

We train all models using PyTorch framework on one NVIDIA A100 GPU, with AdamW optimizer with an exponential learning rate decay. All models are trained with cross-entropy loss combined with Dice loss for 150 epochs with 5 epochs warm up, except SwinUNet, VT-UNet and UNETR, which are trained for 400 epochs. For 3D models, each image can be sampled multiple times to make sure every epoch has 200 iterations. The initial learning rate of 2D models are 0.0005 while 0.001 for 3D models. We use batch size 32 for 2D models and 3 for 3D models. Data augmentation are applied on the fly during training, including random rotation, translation, scaling, brightness shift, Gaussian noise and random crop.

2) *Evaluation Metrics*: We use two types of metric to evaluate all models. The Dice similarity coefficient (DSC) which evaluates the overlap of the predicted and ground truth segmentation map:

$$DSC = \frac{2|P \cap G|}{|P| + |G|}, \quad (6)$$

where P indicates the predicted segmentation map and G denotes the ground truth.

Hausdorff distance (HD) which measures the largest symmetrical distance between two segmentation maps:

$$d_H(P, G) = \max \left\{ \sup_{p \in P} \inf_{g \in G} d(p, g), \sup_{g \in G} \inf_{p \in P} d(p, g) \right\}, \quad (7)$$

where $d(\cdot)$ represents the Euclidean distance, sup and inf denote supremum and infimum, respectively. We employ 95% HD to eliminate the impact of a very small subset of the outliers.

C. Experiments on large cardiac MRI dataset

To compare the performance of CNN based and Transformer based model in different scale of data amount, we shuffle the collected large cardiac dataset and train all models with 5%, 10%, 40%, 70%, or 100% of the whole dataset, and test the trained models on the same M&Ms testing set.

1) *Comparison Methods*: In this experiment, we compare the proposed UTNetV2 with multiple CNN based and Transformer based segmentation models in both 2D and 3D setting. For CNN models, we compare with:

- UNet [14] is a well-known segmentation model. We implement the original UNet in both 2D and 3D setting, which employ double convolution layers in every level.
- UNet++ [20] introduces nested connections to UNet for better high-level and low-level feature fusion.
- Attention UNet [26] uses an attention gating model to let model to focus on the target structures.
- ResUNet uses residual block as the building block of the UNet for better performance and faster convergence.

- Dual attention [23] employs a position and a channel attention for spatial and semantic feature aggregation. We implement it on top of ResUNet backbone on the lowest resolution feature maps.
- ResNet50-UNet [49] uses ResNet-50 as the encoder while the decoder is the same with UNet.
- VNet [50] is a variant of UNet for 3D image segmentation.

For Transformer or hybrid models, we compare with:

- TransUNet [6] uses a R50-ViT [1], which builds ViT on top of a ResNet-50 backbone, as the encoder and employs a UNet decoder for 2D medical image segmentation
- SwinUNet [7] uses a Swin Transformer block in both the encoder and decoder for 2D medical image segmentation.
- UNETR [8] uses a ViT-like structure as the encoder and use a CNN decoder for 3D medical image segmentation.
- VT-UNet-B [9] adapts SwinTransformer block to 3D in both encoder and decoder for volumetric segmentation.
- UTNetV1 [32] employ interleaved convolutional layers, Transformer blocks and efficient attention.

2) *Quantitative Results*: Table II. shows the Dice score of each model in difference training data scale. As the amount of training data increases, the performance of all models has been improved, of which the improvement of from 5% to 40% is more pronounced, while the performance improvement brought by further increasing training data is gradually saturated. It is worth noting that CNN-based models can also achieve excellent performance when using the same training techniques to Transformer models. Under the small-scale training data of 5% and 10%, ResUNet and ResUNet-based Dual attention, as well as Res50-UNet, have achieved good results. TransUNet has achieved decent performance even if trained from scratch, credit to the ResNet50 in the encoder. Using pre-training weights can slightly increase the performance. However, TransUNet does not outperform Res50-UNet by much though with much more parameters. Similarly, Dual Attention has only negligible advantage over ResUNet, while UNETR's results are not good, as its encoder follows ViT structure that process directly on $16 \times$ down-sampled image patches. This indicating that modeling long-range relationship on $16 \times$ down-sampled token map gain limited advantages for the fine-grain details in segmentation tasks. SwinUNet uses a pure hierarchical Transformer architecture. The performance is much lower than the CNN models in this small dataset when training from scratch. Nevertheless, it outperforms CNN models in the case of using pre-trained weights, which indicates that in the case of a low-data regime, using the weights pre-trained on a large-scale natural image dataset can improve the performance and generalization of Transformer on medical images. As a comparison, UTNetV1 using a hybrid model achieves is slightly better than SwinUNet. UTNetV2, with a hybrid architecture specially designed for medical imaging, although has a small number of parameters and Flops, the performance

TABLE II
DICE SCORE OF EXPERIMENTS ON LARGE CARDIAC MRI DATASET

	Arch.	Models	#Param	FLOPs	5%	10%	40%	70%	100%
2D	CNN	UNet [14]	7.8M	14.0G	85.86	86.61	87.49	87.97	88.15
		Attn UNet [48]	8.2M	14.4G	85.59	86.69	87.78	88.09	88.42
		UNet++ [20]	9.2M	34.7G	85.86	86.62	87.95	88.18	88.51
		ResUNet	19.6M	32.9G	85.93	86.62	87.78	88.28	88.58
		ResUNet+DualAttn [23]	21.0M	33.3G	85.95	86.61	87.82	88.31	88.61
		Res50-UNet [49]	27.5M	33.9G	85.44	86.84	88.09	88.39	88.52
	Transformer/Hybrid	TransUNet [6]	105.3M	38.6G	85.48	86.69	87.42	88.34	88.60
		TransUNet†	105.3M	38.5G	85.74	86.88	87.95	88.32	88.55
		SwinUNet [7]	41.4M	11.8G	79.08	82.19	85.13	85.71	86.59
		SwinUNet†	41.4M	11.8G	86.11	87.06	87.95	88.31	88.49
		UTNetV1 [32]	12.8M	22.4G	86.16	87.10	88.11	88.39	88.69
		UTNetV2	12.8M	15.5G	86.71	87.59	88.54	88.61	88.95
3D	CNN	UNet [14]	16.3M	169.5G	84.97	85.68	86.51	87.22	87.89
		ResUNet	39.4M	445.4G	86.01	86.57	87.79	88.32	88.53
		VNet [50]	45.6M	334.2G	84.96	85.72	86.61	87.62	88.01
	Transformer/Hybrid	UNETR [8]	92.4M	42.2G	79.64	80.94	82.22	83.31	84.01
		VT-UNet-B [9]	20.3M	152.3G	78.88	82.02	85.24	86.27	87.01
		VT-UNet-B†	20.3M	152.3G	86.21	86.95	87.92	88.33	88.54
		UTNetV1	17.9M	431.2G	86.34	87.34	88.22	88.31	88.83
		UTNetV2	15.3M	196.1G	86.84	87.62	88.51	88.66	89.01

† indicates the model is initialized with pre-trained weights on ImageNet21K.

The Flops are measured with 256×256 input size for 2D models, while $16 \times 192 \times 192$ for 3D models

goes a step further and far exceeds other models even without large-scale pre-training weights

Under large-scale training data settings, such as 70% and 100%. The TransUNet trained from scratch outperforms the model with pre-trained weights. For a pure Transformer model SwinUNet, training from scratch is still lower than using pre-training weights. However, even with pre-training weights, SwinUNet does not outperform the best CNN model, similar for VT-UNet, which shows that large-scale natural images pre-training weights do not yield advantages on large-scale medical image segmentation datasets due to the domain gap. The dataset with size of the 1418 MRI images is not large enough to support the pure Transformer-based model to be trained from scratch and show higher potential capacity. Our proposed UTNetV2 combines the strength of CNN and Transformer and achieve a better result.

The performance of 2D and 3D is close due to the large slice thickness of cardiac MRI. The training time of 3D models and the difficulty of hyper-parameter tuning are much greater than that of 2D models. For example, 3D UNet still uses the same double convolution, but it is more difficult to train and worse than 2D UNet. However, 3D ResUNet uses residual connections in the building block, resulting in better gradient flow, and usually has better results than 2D ResUNet. The 3D version of the proposed UTNetV2 also generally has better performance than 2D due to better combining inter-slice information.

3) *Robustness Analysis*: The M&Ms test set, which contains data from four MRI vendors (A, B, C, D), where data of vendor A and B are included in the training set, while data of vendor C and D are not. We can use it to evaluate the robustness of the models, as there are certain domain gaps between images from different vendors. The performance of several 2D models using 100% dataset on all

TABLE III
ROBUSTNESS ANALYSIS.

	A	B	C	D
ResUNet	89.02	89.66	88.31 ($\downarrow 1.03$)	87.33 ($\downarrow 2.01$)
TransUNet	88.97	89.44	88.01 ($\downarrow 1.19$)	88.00 ($\downarrow 1.20$)
SwinUNet	88.60	89.41	88.41 ($\downarrow 0.60$)	87.55 ($\downarrow 1.46$)
UTNetV2	89.23	89.61	88.65 ($\downarrow 0.77$)	88.31 ($\downarrow 1.11$)

The number in the brackets of C and D indicates performance drop compared to the average of A and B.

four domains are presented in Table III. Compared with other approaches, UTNetV2 has a small advantage in the domains A and B that exist in the training set, but has a greater advantage in the unseen domains of C and D. UTNetV2 has a small performance drop on unseen domain C and D, which demonstrated its good robustness to domain gap.

4) *Conclusion*: Through these experiments, we can draw the following conclusions:

- Under small-scale datasets, CNNs can converge faster and perform better due to more inductive bias. The performance of pure Transformer models trained from scratch is lower than that of the CNN models.
- Pre-training weights based on large-scale natural image datasets can improve the performance of Transformer on small-scale medical image datasets. However, due to the gap between medical and natural images, this performance gain weakens with the increase of medical image dataset size.
- Modeling long-range relationship on excessively down-sampled token map, e.g. $16\times$, gains limited advantages for the fine-grain details in segmentation tasks.
- The hybrid model combines the strength of both CNN and Transformer, which usually converges quickly on small-scale datasets and has excellent potential capacity

on large-scale datasets.

- Although the training time and parameter tuning difficulty of the 3D models are greater than that of the 2D models, they usually have better performance than the 2D models due to the ability to combine inter-slice volumetric information.

D. Experiments on ACDC and BTCV

To fair comparison with other state-of-the-art methods, we further conduct experiments on ACDC and BTCV dataset. This experiments aim at verifying the performance of our proposed method under different modalities and different target anatomical structures. Since the scales of these datasets are relatively small, all following results are obtained by randomly shuffling the datasets and five-fold cross-validation.

1) *ACDC*: Table IV shows the mean and standard deviation of the Dice score and 95% Hausdorff distance of the five folds.

The baseline UNet achieved a average DSC of 91.05. UNet++ with more high- and low-level fusion, ResUNet with residual connection, or attention UNet with attention gated mechanism all have certain performance improvements compared to the original UNet. In contrast, the R50-ViT-based TransUNet is not better than the CNN-based models, even initialized with pre-trained weights, which further verifies that long-range modeling on low-resolution feature maps can gain limited advantage for the detailed segmentation. SwinUNet, VT-UNet and UNETR are trained for 400 epochs, while all other models are only trained for 150 epochs, as the convergence speed of the Transformers are much slower than CNNs. It can be seen that without using a pre-trained weights, the accuracy of SwinUNet and VT-UNet are much lower than other models on this small dataset due to the lack of inductive bias. They does not outperform other CNN models, even with pre-trained weights, which seems contradictory to the conclusion from the large cardiac dataset. This is because the source of ACDC is not as diverse as the large cardiac dataset, as there is no data from multiple vendors and domains so that CNNs can fit faster during the training process, thereby offsetting the generalization advantage brought by the pre-training weights. The proposed UTNetV2 is superior to all CNN and Transformer-based models in Dice score and Hausdorff distance metrics.

As residual connections are vital in gradient flow and faster training for the 3D models, we use 3D ResUNet as the baseline. Compared with the 2D model, both 3D ResUNet and 3D attention ResUNet have slightly improved Dice score and 95HD. More importantly, the standard deviations of 3D models are much smaller than that of 2D models, which demonstrates that the robustness of 3D models is better than 2D models. UNETR still perform not well, which shows shortcomings of ViT-like structure on dense prediction tasks such as segmentation tasks due to excessive down-sampling in the patchify process. The 3D UTNetV2 is ahead of other models in both metrics, and the standard deviation in the 5-fold cross-validation is also small, showing good performance, robustness, and generalization.

Fig. 2 shows the segmentation visualization on ACDC dataset. The upper row shows a normal case, most models can achieve decent segmentation with complete structure and errors only appear in edge details. However, slices next to the valves or the apex of the ventricle are more difficult to segment. The bottom row of Fig. 2 shows a hard case. 2D ResUNet and TransUNet are prone to have disconnected MYO, 3D UNETR and VT-UNet have some errors in the RV. The proposed UTNetV2 has good results in both 2D and 3D setting.

2) *BTCV*: Due to the small slice thickness and large image size of the abdomen CT, the performance of the 2D models is much lower than 3D models. Therefore, we only report the average performance of all organs from the 3D models in BTCV dataset, see in Table V. All models use the same training strategy and the mean and standard deviation of 5-fold cross-validation are presented. Our UTNetV2 achieved the best performance in both DSC and 95HD. The performance of UNETR and VT-UNet is lower than well-trained CNN even with much longer training epochs (400 v.s. 150) in the small dataset. The performance of UNETR in our training framework is lower than what the author reported, which might because we don't use extensive model ensemble for evaluation.

E. Ablation Study

We conduct the ablation study of the proposed method on ACDC dataset in 2D setting.

1) *Effect of each proposed component*: We first conduct experiments on the contribution of each component to the final performance, see in 3 (a). Our baseline is the CNN model ResUNet. We first test UTNetV1, that is, adding an efficient attention block on the basis of ResUNet. Compared with the baseline, UTNetV1 has a 0.27 Dice score improvement. We further add the convolution projection and feed-forward network, which brought a performance improvement of 0.13 and 0.06, respectively. Then we replace the efficient attention in UTNetV1 with B-MHA. The concise semantic map retain more useful tokens after reduction, and the performance further increases by 0.11. Finally, we added multi-scale fusion to further improve the performance by 0.10. We also attempted add position information the attention computation via relative position embedding, but it did not improve performance. This is because the proposed B-MHA greatly reduces the number of tokens, and the role of relative position between tokens and the semantic map is weakened. In addition, our proposed convolution projection and feed-forward network can inherently introduce the concept of relative position to Transformer for a certain extent.

2) *Effect of the applied level of the Transformer block*: Fig. 3 (c) shows the performance of different transformer block positions. The number in the x-axis indicates the level where the B-MHA Transformer block is places. As the level goes up, the self-attention can gather more fine-grained detail information with increased performance. However, the curve saturates when adding to the $2 \times$ down-sampling resolution. We reason this as the very shallow layer tends to be more

TABLE IV
RESULTS ON THE ACDC DATASET.

Model	RV		MYO		LV		AVG	
	DSC	95HD	DSC	95HD	DSC	95HD	DSC	95HD
UNet	90.10 \pm 1.21	5.91 \pm 1.37	88.86 \pm 0.32	2.49 \pm 0.50	94.17 \pm 1.07	2.94 \pm 0.76	91.05 \pm 0.69	3.78 \pm 0.74
UNet++	90.00 \pm 1.19	6.91 \pm 2.31	89.31 \pm 0.43	2.42 \pm 0.31	94.33 \pm 1.01	2.83 \pm 0.45	91.21 \pm 0.72	4.06 \pm 0.79
ResUNet	90.44 \pm 1.08	5.53 \pm 1.00	89.13 \pm 0.43	2.53 \pm 0.39	94.16 \pm 1.09	3.08 \pm 0.85	91.25 \pm 0.66	3.71 \pm 0.62
Attn UNet	90.48 \pm 1.08	5.48 \pm 0.92	88.93 \pm 0.33	2.82 \pm 0.77	94.13 \pm 1.36	3.25 \pm 1.31	91.18 \pm 0.80	3.85 \pm 0.91
TransUNet	89.66 \pm 1.46	6.22 \pm 1.46	88.07 \pm 0.39	3.08 \pm 1.21	93.98 \pm 0.99	3.28 \pm 1.42	90.57 \pm 0.74	4.19 \pm 1.08
TransUNet †	89.78 \pm 1.29	6.31 \pm 1.32	88.74 \pm 0.58	3.06 \pm 1.31	94.03 \pm 1.29	3.38 \pm 1.45	90.85 \pm 0.97	4.25 \pm 1.29
SwinUNet	81.81 \pm 3.27	13.51 \pm 2.35	81.18 \pm 2.86	6.54 \pm 3.44	90.01 \pm 2.50	7.80 \pm 3.60	84.34 \pm 2.77	9.28 \pm 2.82
SwinUNet †	90.34 \pm 1.11	5.44 \pm 1.05	88.70 \pm 0.47	3.11 \pm 1.39	94.05 \pm 1.40	3.78 \pm 2.21	91.03 \pm 0.91	4.11 \pm 1.52
UTNetV1	90.41 \pm 1.03	5.59 \pm 0.95	89.15 \pm 0.58	2.54 \pm 0.57	94.39 \pm 1.24	2.96 \pm 1.12	91.32 \pm 0.81	3.69 \pm 0.79
UTNetV2	90.96 \pm 0.64	5.27 \pm 0.54	89.63 \pm 0.36	2.49 \pm 0.48	94.59 \pm 1.09	2.91 \pm 0.85	91.73 \pm 0.58	3.55 \pm 0.54
ResUNet	89.77 \pm 0.29	5.04 \pm 0.27	88.95 \pm 0.17	2.54 \pm 0.26	95.16 \pm 0.22	2.77 \pm 0.20	91.29 \pm 0.21	3.45 \pm 0.23
Attn ResUNet	90.01 \pm 0.20	5.05 \pm 0.32	89.09 \pm 0.16	2.39 \pm 0.18	95.22 \pm 0.09	2.73 \pm 0.08	91.44 \pm 0.08	3.39 \pm 0.15
UNETR	84.52 \pm 0.26	9.06 \pm 3.08	84.36 \pm 0.37	3.30 \pm 1.89	92.57 \pm 0.17	4.10 \pm 0.45	87.15 \pm 0.19	5.48 \pm 1.13
VT-UNet-B	80.44 \pm 2.92	11.09 \pm 1.78	80.71 \pm 2.07	5.24 \pm 2.02	89.53 \pm 1.99	6.32 \pm 2.95	83.56 \pm 2.32	5.55 \pm 2.25
VT-UNet-B †	89.44 \pm 0.19	5.02 \pm 0.18	88.42 \pm 0.07	2.14 \pm 0.02	95.53 \pm 0.03	2.19 \pm 0.05	91.13 \pm 0.08	3.12 \pm 0.07
UTNetV1	89.92 \pm 0.28	5.03 \pm 0.25	89.25 \pm 0.18	2.41 \pm 0.16	95.40 \pm 0.15	2.69 \pm 0.08	91.52 \pm 0.18	3.37 \pm 0.09
UTNetV2	90.95 \pm 0.28	4.47 \pm 0.32	89.71 \pm 0.08	2.23 \pm 0.10	95.76 \pm 0.06	2.55 \pm 0.07	92.14 \pm 0.12	3.08 \pm 0.11

The top table shows the results of 2D models, and the bottom table shows 3D models.

† indicates the model is initialized with pre-trained weights on ImageNet21K.

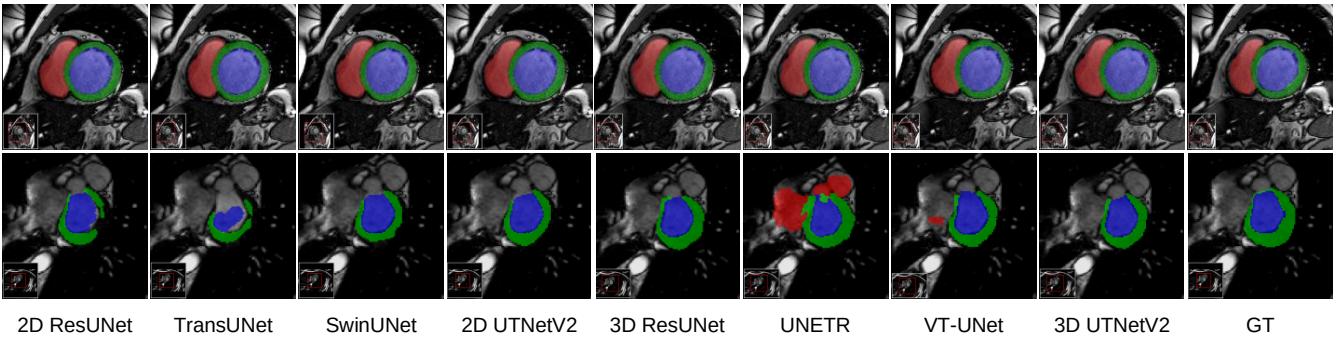


Fig. 2. The segmentation visualization on ACDC. The upper shows the results of a normal case, while the bottom shows a hard case.

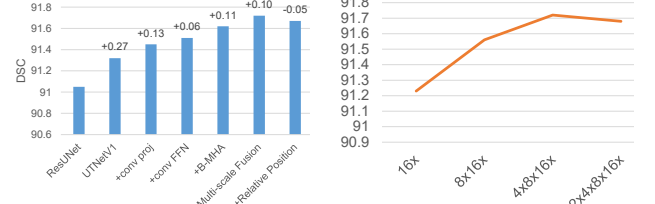
TABLE V
RESULTS ON BTCV DATASET.

Model	DSC	95HD
ResUNet	83.82 \pm 2.30	16.61 \pm 4.71
VNet	82.72 \pm 2.98	18.27 \pm 5.77
UNETR	81.10 \pm 3.55	19.21 \pm 4.21
VT-UNet †	82.33 \pm 2.01	16.92 \pm 3.92
UTNetV1	83.93 \pm 2.23	16.45 \pm 4.55
UTNetV2	85.14 \pm 1.57	15.78 \pm 2.87

focused on local texture, where global context information is not informative anymore.

V. DISCUSSION

1) *Why UTNetV2 works:* The key advances of our approach fall into two folds. The first is the design of the hybrid architecture, which combines the advantages of both CNN and Transformer. In the shallow layers of the network, UTNetV2 uses CNN stem to extract local features while reducing the resolution. In the middle and deep layers of the model, we use the proposed B-MHA Transformer block to enhance the representation. By introducing the convolution projection and feed-forward network, the proposed B-MHA



(a) The contribution of each component to the final performance. (b) Effect of Transformer block level.

Fig. 3. Ablation Study

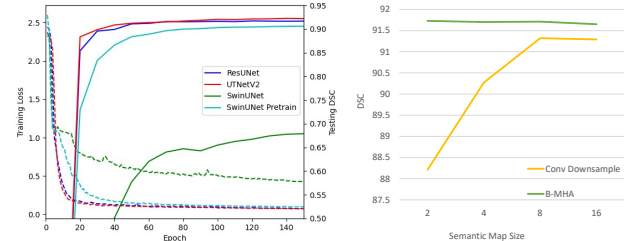
Transformer block can model both long-range and local relationship. Fig. 4 shows the training loss and test DSC of the pure CNN model ResUNet, the pure Transformer model SwinUNet, and UTNetV2 on one fold of ACDC dataset. All models were trained for 150 epochs using the same training strategy and optimizer. It should be noted that SwinUNet can achieve better performance when trained with more epochs (the results we report in Table III are trained for 400 epochs), but to compare the convergence speed, we let all models use the same training strategy. SwinUNet converges very slowly without pre-training weights. Due to the lack of inductive

bias, the performance of the model cannot be exerted at all on small-scale medical image datasets. Even with pre-training weight, it still converges slower than ResUNet. UTNetV2 with hybrid architecture can converge as quickly as CNN without pre-training weights in small-scale medical datasets.

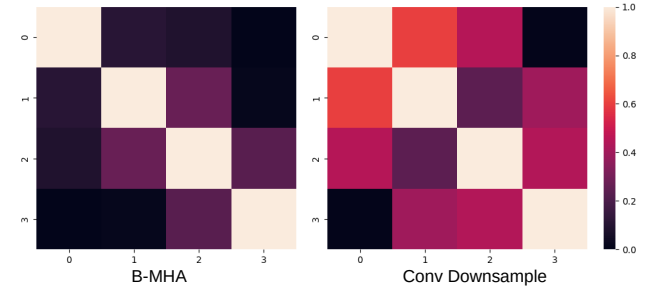
Secondly, our proposed bidirectional attention, which reduces the number of tokens, thus reducing the complexity to linear. Its nonlinear dimensional reduction can make the compressed tokens are the most useful ones. We conducted experiments on the size of the semantic map from convolutional down-sampling and the proposed B-MHA module, see Fig. 4 (b). It can be seen that for efficient attention using convolution reduction, as the size of the semantic map decreases, the segmentation accuracy drops a lot. This is because linear compression cannot effectively retain valid tokens, resulting in information loss and degraded performance. Our proposed B-MHA still has high performance even when the semantic map size is 2. To further verify the above explanation, we calculate the correlation, measured with cosine similarity, between the compressed tokens in the size-2 semantic map from B-MHA and convolutional down-sampling respectively. The heatmap of the cosine similarity matrix is shown in Fig. 4 (c). For the convenience of visualization, we take the absolute value of the cosine similarity. It can be seen that the similarity between the tokens compressed by B-MHA is very low, while the convolution down-sampling is much higher. This experiment demonstrates that the tokens compressed by B-MHA are more orthogonal, and retain less redundant information between each other. In contrast, convolution down-sampling has more redundancy and lower compression efficiency, and cannot guarantee that valid information is preserved when the semantic map is small. Since the ACDC dataset only has 4 categories, and the multiple heads in the attention can make each head focus on different areas of the image, semantic map with size 2 (4 tokens) is still enough to retain effective information. In addition, since the semantic map in B-MHA is preserved and further updated in the next Transformer block, the semantic map is gradually updated and refined. In contrast, Efficient attention requires compression in each Transformer block, and all previous information is discarded. Therefore the proposed B-MHA is also better when semantic map size is large.

The attention maps of some test samples are shown in the Fig. 5. The whiter means the higher attention weight. Each column represents the attention map corresponding to the token in different positions in the semantic map. It can be seen that the token in the second column corresponds to the background, the third column corresponds to RV, the fourth column corresponds to LV, and the fifth column focus on MYO. The attention map shows that different tokens in the semantic map can aggregate information from different structure globally according to the attention, so that it can better model the long-range relationship. This attention map also brings interpretability to the proposed model for a certain extent.

2) *Transformer Pre-training*: Pre-training is highly desired for Transformer training in NLP [51] and CV [1] tasks,



(a) Converge analysis. Solid line: DSC. (b) Effect of semantic map size. Dashed line: Training loss.



(c) Correlation of token pairs in the compressed semantic map with size 2.

Fig. 4. Discussion of UTNetV2

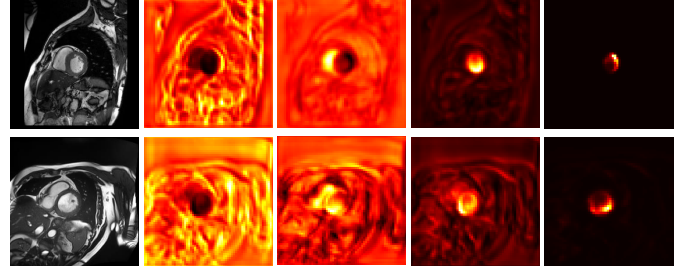


Fig. 5. The attention map visualization.

as Transformer models demonstrate higher model capacity under large-scale pre-training. Yet its application in the medical image field is non-trivial. The typical characteristics of medical images are: there are many tasks, the gap between tasks is huge, and the amount of data for each task is small. In contrast, the domain gaps of different NLP tasks are small, as the corpus and grammar under different tasks and datasets are consistent. Therefore pre-training on large-scale dataset and then fine-tuning on downstream tasks is naturally suitable for NLP area. However, for medical imaging, the domain shift is significant. The appearance, texture and statistics vary greatly between different modalities. This domain gap makes the pre-trained weights on one modality can not generalize well to other modalities. In addition, the pre-training of Transformer usually requires large-scale data. In natural images, even the ImageNet-1k with 1.2M images dataset is regarded as a small-scale dataset, and the ImageNet-21k with 14M images is regarded as a large-scale dataset. However, it is almost impossible to obtain such a large pre-training dataset due to image acquisition difficulty, patient privacy, and high annotation cost. In general, large-scale pre-training

on medical images is still difficult, and there are many problems to be solved. In contrast, the proposed UTNetV2 has fast convergence under small datasets and higher capacity under large datasets without pre-training weights.

3) *CNN v.s. Transformer*: Recently, a lot of work has been done using Transformer in the field of medical imaging, and it seems that Transformer can completely surpass and replace CNNs. However, this is not actually the case in our experiments. In the small dataset setting, CNN can quickly converge to a good performance due to its inherent design, while Transformer without specific design cannot stably surpass CNN even with much more training iterations and pre-train weights. Recent work also shows that well-designed CNNs can outperform Transformers even when trained at large-scale [12]. Therefore, in our opinion, these two are not opposites. Credit to its structure, CNN naturally has inductive bias, does not require large amount of training data, suitable for extracting local features, and has less computational effort when processing high-resolution images. On the other hands, Transformer has no inductive bias, which is learned from scratch during large-scale data training. It has a higher potential capacity under large-scale training and is suitable for extracting long-distance relationships. Therefore, for medical image tasks, combining the advantages of both and avoid the defects of both is a promising way to design a better model. Hopefully, our experiments and the proposed hybrid UTNetV2 structure can shed a light on the future model design directions.

4) *Limitation*: This work aims at designing a model that suitable for medical image segmentation tasks. Although the proposed UTNetV2 can achieve superior results on both small-scale and large-scale medical image datasets, we current only focus on supervised learning setting. In the future, we will evaluate the performance, capacity, and scalability on larger-scale datasets in self-supervised pre-training, or semi-supervised setting to ease the requirement of annotations. In addition, we currently only apply UTNetV2 on medical image segmentation tasks, however, its excellent properties make it a general backbone for dense prediction tasks. We will explore UTNetV2 on more tasks in the future, such as registration, detection, reconstruction, etc.

VI. CONCLUSION

In this study, we have presented a hybrid architecture: UTNetV2, which combines the strength of Transformer and CNN models for medical image segmentation. We introduce convolution projection and feed-forward network to Transformer block for more inductive bias and better local relationship modeling while maintaining the merits of vanilla Transformer for long-range relationship modeling. A bidirectional attention is proposed and reduces the complexity of attention to linear. Multi-scale feature fusion is also incorporated to enhance the segmentation. We demonstrated that the proposed UTNetV2 achieved superior performance across multiple tasks in 2D and 3D setting without pre-training weights. Furthermore, we provide a codebase for fair comparison between CNN models and Transformer

architectures in a variety of medical image segmentation tasks. Hope this codebase can serves as a solid baseline for the future medical image model design.

REFERENCES

- [1] A. Dosovitskiy, L. Beyer, A. Kolesnikov, D. Weissenborn, X. Zhai, T. Unterthiner, M. Dehghani, M. Minderer, G. Heigold, S. Gelly *et al.*, “An image is worth 16x16 words: Transformers for image recognition at scale,” *arXiv preprint arXiv:2010.11929*, 2020.
- [2] Z. Dai, H. Liu, Q. V. Le, and M. Tan, “Coatnet: Marrying convolution and attention for all data sizes,” *arXiv preprint arXiv:2106.04803*, 2021.
- [3] H. Zhao, J. Shi, X. Qi, X. Wang, and J. Jia, “Pyramid scene parsing network,” in *Proceedings of the IEEE conference on computer vision and pattern recognition*, 2017, pp. 2881–2890.
- [4] F. Yu and V. Koltun, “Multi-scale context aggregation by dilated convolutions,” *arXiv preprint arXiv:1511.07122*, 2015.
- [5] Y. Gao, R. Huang, Y. Yang, J. Zhang, K. Shao, C. Tao, Y. Chen, D. N. Metaxas, H. Li, and M. Chen, “Focusnetv2: Imbalanced large and small organ segmentation with adversarial shape constraint for head and neck ct images,” *Medical Image Analysis*, vol. 67, p. 101831, 2021.
- [6] J. Chen, Y. Lu, Q. Yu, X. Luo, E. Adeli, Y. Wang, L. Lu, A. L. Yuille, and Y. Zhou, “Transunet: Transformers make strong encoders for medical image segmentation,” *arXiv preprint arXiv:2102.04306*, 2021.
- [7] H. Cao, Y. Wang, J. Chen, D. Jiang, X. Zhang, Q. Tian, and M. Wang, “Swin-unet: Unet-like pure transformer for medical image segmentation,” *arXiv preprint arXiv:2105.05537*, 2021.
- [8] A. Hatamizadeh, Y. Tang, V. Nath, D. Yang, A. Myronenko, B. Landman, H. Roth, and D. Xu, “Unetr: Transformers for 3d medical image segmentation,” *arXiv preprint arXiv:2103.10504*, 2021.
- [9] H. Peiris, M. Hayat, Z. Chen, G. Egan, and M. Harandi, “A volumetric transformer for accurate 3d tumor segmentation,” *arXiv preprint arXiv:2111.13300*, 2021.
- [10] Z. Liu, Y. Lin, Y. Cao, H. Hu, Y. Wei, Z. Zhang, S. Lin, and B. Guo, “Swin transformer: Hierarchical vision transformer using shifted windows,” *arXiv preprint arXiv:2103.14030*, 2021.
- [11] R. Wightman, H. Touvron, and H. Jégou, “Resnet strikes back: An improved training procedure in timm,” *arXiv preprint arXiv:2110.00476*, 2021.
- [12] Z. Liu, H. Mao, C.-Y. Wu, C. Feichtenhofer, T. Darrell, and S. Xie, “A convnet for the 2020s,” *arXiv preprint arXiv:2201.03545*, 2022.
- [13] J. Long, E. Shelhamer, and T. Darrell, “Fully convolutional networks for semantic segmentation,” in *Proceedings of the IEEE conference on computer vision and pattern recognition*, 2015, pp. 3431–3440.
- [14] O. Ronneberger, P. Fischer, and T. Brox, “U-net: Convolutional networks for biomedical image segmentation,” in *International Conference on Medical image computing and computer-assisted intervention*. Springer, 2015, pp. 234–241.
- [15] L.-C. Chen, G. Papandreou, I. Kokkinos, K. Murphy, and A. L. Yuille, “Deeplab: Semantic image segmentation with deep convolutional nets, atrous convolution, and fully connected crfs,” *IEEE transactions on pattern analysis and machine intelligence*, vol. 40, no. 4, pp. 834–848, 2017.
- [16] F. Yu, V. Koltun, and T. Funkhouser, “Dilated residual networks,” in *Proceedings of the IEEE conference on computer vision and pattern recognition*, 2017, pp. 472–480.
- [17] L.-C. Chen, Y. Yang, J. Wang, W. Xu, and A. L. Yuille, “Attention to scale: Scale-aware semantic image segmentation,” in *Proceedings of the IEEE conference on computer vision and pattern recognition*, 2016, pp. 3640–3649.
- [18] T.-Y. Lin, P. Dollár, R. Girshick, K. He, B. Hariharan, and S. Belongie, “Feature pyramid networks for object detection,” in *Proceedings of the IEEE conference on computer vision and pattern recognition*, 2017, pp. 2117–2125.
- [19] L.-C. Chen, G. Papandreou, F. Schroff, and H. Adam, “Rethinking atrous convolution for semantic image segmentation,” *arXiv preprint arXiv:1706.05587*, 2017.
- [20] Z. Zhou, M. M. R. Siddiquee, N. Tajbakhsh, and J. Liang, “Unet++: A nested u-net architecture for medical image segmentation,” in *Deep learning in medical image analysis and multimodal learning for clinical decision support*. Springer, 2018, pp. 3–11.

[21] F. Yu, D. Wang, E. Shelhamer, and T. Darrell, “Deep layer aggregation,” in *Proceedings of the IEEE conference on computer vision and pattern recognition*, 2018, pp. 2403–2412.

[22] S. Woo, J. Park, J.-Y. Lee, and I. S. Kweon, “Cbam: Convolutional block attention module,” in *Proceedings of the European conference on computer vision (ECCV)*, 2018, pp. 3–19.

[23] J. Fu, J. Liu, H. Tian, Y. Li, Y. Bao, Z. Fang, and H. Lu, “Dual attention network for scene segmentation,” in *Proceedings of the IEEE/CVF Conference on Computer Vision and Pattern Recognition*, 2019, pp. 3146–3154.

[24] Z. Huang, X. Wang, L. Huang, C. Huang, Y. Wei, and W. Liu, “Ccnet: Criss-cross attention for semantic segmentation,” in *Proceedings of the IEEE/CVF International Conference on Computer Vision*, 2019, pp. 603–612.

[25] P. F. Christ, M. E. A. Elshaer, F. Ettlinger, S. Tatavarty, M. Bickel, P. Bilic, M. Rempfler, M. Armbrester, F. Hofmann, M. D’Anastasi *et al.*, “Automatic liver and lesion segmentation in ct using cascaded fully convolutional neural networks and 3d conditional random fields,” in *International Conference on Medical Image Computing and Computer-Assisted Intervention*. Springer, 2016, pp. 415–423.

[26] O. Oktay, J. Schlemper, L. L. Folgoc, M. Lee, M. Heinrich, K. Misawa, K. Mori, S. McDonagh, N. Y. Hammerla, B. Kainz *et al.*, “Attention u-net: Learning where to look for the pancreas,” *arXiv preprint arXiv:1804.03999*, 2018.

[27] J. Yi, P. Wu, M. Jiang, Q. Huang, D. J. Hoepfner, and D. N. Metaxas, “Attentive neural cell instance segmentation,” *Medical image analysis*, vol. 55, pp. 228–240, 2019.

[28] T. Brosch, L. Y. Tang, Y. Yoo, D. K. Li, A. Traboulsee, and R. Tam, “Deep 3d convolutional encoder networks with shortcuts for multiscale feature integration applied to multiple sclerosis lesion segmentation,” *IEEE transactions on medical imaging*, vol. 35, no. 5, pp. 1229–1239, 2016.

[29] C. Tan, L. Zhao, Z. Yan, K. Li, D. Metaxas, and Y. Zhan, “Deep multi-task and task-specific feature learning network for robust shape preserved organ segmentation,” in *2018 IEEE 15th International Symposium on Biomedical Imaging (ISBI 2018)*. IEEE, 2018, pp. 1221–1224.

[30] H. Wu, B. Xiao, N. Codella, M. Liu, X. Dai, L. Yuan, and L. Zhang, “Cvt: Introducing convolutions to vision transformers,” *arXiv preprint arXiv:2103.15808*, 2021.

[31] H. Wang, Y. Zhu, B. Green, H. Adam, A. Yuille, and L.-C. Chen, “Axial-deeplab: Stand-alone axial-attention for panoptic segmentation,” in *European Conference on Computer Vision*. Springer, 2020, pp. 108–126.

[32] Y. Gao, M. Zhou, and D. N. Metaxas, “Utnet: a hybrid transformer architecture for medical image segmentation,” in *International Conference on Medical Image Computing and Computer-Assisted Intervention*. Springer, 2021, pp. 61–71.

[33] W. Wang, E. Xie, X. Li, D.-P. Fan, K. Song, D. Liang, T. Lu, P. Luo, and L. Shao, “Pyramid vision transformer: A versatile backbone for dense prediction without convolutions,” in *Proceedings of the IEEE/CVF International Conference on Computer Vision*, 2021, pp. 568–578.

[34] Z. Cai, Q. Fan, R. S. Feris, and N. Vasconcelos, “A unified multi-scale deep convolutional neural network for fast object detection,” in *European conference on computer vision*. Springer, 2016, pp. 354–370.

[35] Y. Chen, Z. Wang, Y. Peng, Z. Zhang, G. Yu, and J. Sun, “Cascaded pyramid network for multi-person pose estimation,” in *Proceedings of the IEEE conference on computer vision and pattern recognition*, 2018, pp. 7103–7112.

[36] J. Tompson, R. Goroshin, A. Jain, Y. LeCun, and C. Bregler, “Efficient object localization using convolutional networks,” in *Proceedings of the IEEE conference on computer vision and pattern recognition*, 2015, pp. 648–656.

[37] A. Lin, B. Chen, J. Xu, Z. Zhang, and G. Lu, “Ds-transunet: Dual swin transformer u-net for medical image segmentation,” *arXiv preprint arXiv:2106.06716*, 2021.

[38] C.-F. Chen, Q. Fan, and R. Panda, “Crossvit: Cross-attention multi-scale vision transformer for image classification,” *arXiv preprint arXiv:2103.14899*, 2021.

[39] J. Wang, K. Sun, T. Cheng, B. Jiang, C. Deng, Y. Zhao, D. Liu, Y. Mu, M. Tan, X. Wang *et al.*, “Deep high-resolution representation learning for visual recognition,” *IEEE transactions on pattern analysis and machine intelligence*, 2020.

[40] A. Vaswani, N. Shazeer, N. Parmar, J. Uszkoreit, L. Jones, A. N. Gomez, L. Kaiser, and I. Polosukhin, “Attention is all you need,” in *NIPS*, 2017.

[41] F. Chollet, “Xception: Deep learning with depthwise separable convolutions,” in *Proceedings of the IEEE conference on computer vision and pattern recognition*, 2017, pp. 1251–1258.

[42] M. Sandler, A. Howard, M. Zhu, A. Zhmoginov, and L.-C. Chen, “Mobilenetv2: Inverted residuals and linear bottlenecks,” in *Proceedings of the IEEE conference on computer vision and pattern recognition*, 2018, pp. 4510–4520.

[43] S. Wang, B. Li, M. Khabsa, H. Fang, and H. Ma, “Linformer: Self-attention with linear complexity,” *arXiv preprint arXiv:2006.04768*, 2020.

[44] O. Bernard, A. Lalande, C. Zotti, F. Cervenansky, X. Yang, P.-A. Heng, I. Cetin, K. Lekadir, O. Camara, M. A. G. Ballester *et al.*, “Deep learning techniques for automatic mri cardiac multi-structures segmentation and diagnosis: is the problem solved?” *IEEE transactions on medical imaging*, vol. 37, no. 11, pp. 2514–2525, 2018.

[45] V. M. Campello, P. Gkontra, C. Izquierdo, C. Martín-Isla, A. Sojoudi, P. M. Full, K. Maier-Hein, Y. Zhang, Z. He, J. Ma *et al.*, “Multi-centre, multi-vendor and multi-disease cardiac segmentation: the m&ms challenge,” *IEEE Transactions on Medical Imaging*, vol. 40, no. 12, pp. 3543–3554, 2021.

[46] “Multi-atlas labeling beyond the cranial vault - workshop and challenge.”

[47] F. Isensee, P. F. Jaeger, S. A. Kohl, J. Petersen, and K. H. Maier-Hein, “nnu-net: a self-configuring method for deep learning-based biomedical image segmentation,” *Nature methods*, vol. 18, no. 2, pp. 203–211, 2021.

[48] J. Schlemper, O. Oktay, M. Schaap, M. Heinrich, B. Kainz, B. Glocker, and D. Rueckert, “Attention gated networks: Learning to leverage salient regions in medical images,” *Medical image analysis*, vol. 53, pp. 197–207, 2019.

[49] K. He, X. Zhang, S. Ren, and J. Sun, “Deep residual learning for image recognition,” in *Proceedings of the IEEE conference on computer vision and pattern recognition*, 2016, pp. 770–778.

[50] F. Milletari, N. Navab, and S.-A. Ahmadi, “V-net: Fully convolutional neural networks for volumetric medical image segmentation,” in *2016 fourth international conference on 3D vision (3DV)*. IEEE, 2016, pp. 565–571.

[51] J. Devlin, M.-W. Chang, K. Lee, and K. Toutanova, “Bert: Pre-training of deep bidirectional transformers for language understanding,” *arXiv preprint arXiv:1810.04805*, 2018.